SPACECRAFT ORBITAL DEBRIS REENTRY AEROTHERMAL ANALYSIS

Wm. C. Rochelle,* Robin E. Kinsey,** Ethan A. Reid,** and Robt. C. Reynolds+
Lockheed Martin, Houston, TX

Nicholas L. Johnson++
NASA/JSC, Houston, TX

Abstract

In the past 40 years, thousands of objects have been placed in Earth orbit and are being tracked. Space hardware reentry survivability must be evaluated to assess risks to human life and property on the ground. The objective of this paper is to present results of a study to determine altitude of demise (burn-up) or survivability of reentering objects. Two NASA/JSC computer codes - Object Reentry Survival Analysis Tool (ORSAT) and Miniature ORSAT (MORSAT) were used to determine trajectories, aerodynamics, aerothermal environment, and thermal response of selected spacecraft components. The methodology of the two codes is presented, along with results of a parametric study of reentering objects modeled as spheres and cylinders. Parameters varied included mass, diameter, wall thickness, ballistic coefficient, length, type of material, and mode of tumbling/spinning. Two fragments of a spent Delta second stage undergoing orbital decay - stainless steel cylindrical propellant tank and titanium pressurization sphere - were evaluated with ORSAT and found to survive entry, as did the actual objects. Also, orbital decay reentry predictions of the Japanese Advanced Earth Observing Satellite (ADEOS) aluminum and nickel box-type components and the Russian COSMOS 954 satellite beryllium cylinders were made with MORSAT. These objects were also shown to survive reentry.

Introduction

Since the launch of Sputnik I, thousands of man-made objects are in orbit around Earth, and at least 9000 larger objects are being tracked by the U. S. Space Command Space Surveillance Network. These objects include active payloads as well as orbital debris - inactive payloads, spent upper stages, operational debris, and fragmentation debris from more than 140 on-orbit explosions. The orbital debris environment is increasing with time and represents an increasing risk to future space programs. Government organizations have been investigating responses to this growing problem.[1]

Two of the measures which have been implemented into NASA safety guidelines[2] are the removal of on-board stored energy at the end of mission life to prevent future accidental explosions and the limitation of the lifetime of debris objects in low Earth orbit to 25 years to prevent future growth of the orbital debris environment by on-orbit collisions. The guideline to restrict the lifetime of orbital debris applies in particular to payloads and upper stages after completion of their mission. The most feasible alternative for programs to adopt in order to implement this guideline is to use atmospheric drag and reentry heating to remove these objects from orbit. Because atmospheric reentry has been adopted as a method to respond to this guideline, it is essential that NASA be able to evaluate and limit the risk associated with these reentry events. Thus, NASA has also adopted a safety guideline for reentry risk.

To predict this risk in a form suitable for consideration during program development, NASA has sponsored a study at NASA/JSC to develop and implement tools to work this problem from early in program development, when design concepts are developed and material usage is being planned, through critical design review, when the evaluation can be made with less uncertainty. The tools described in this paper were developed during this project and are part of an international effort to better understand the problem of reentry survivability.

The objective of this paper is to present an evaluation of orbital debris reentry to determine the point of demise (burn-up) or survivability of the object. Two NASA/JSC computer codes - Object Reentry Survival Analysis Tool (ORSAT)[3] and Miniature ORSAT (MORSAT)[4] - were used to determine the trajectories, aerodynamics, aerothermal environment, and thermal response of selected spacecraft components. These codes have been validated[5,6] by providing good comparison of predicted demise altitude with the flight-measured value of a Sandia fuel rod undergoing orbital decay. With these codes, the trajectory of a parent body is assumed to decay down to an altitude where this body breaks into smaller fragments. These fragments then

*Group Lead, Advanced Systems Group
**Cooperative Engineering Student, Adv. Sys. Grp.
+Project Manager, Orbital Debris Projects
++Senior Scientist for Orbital Debris, Space Science Br.

follow a trajectory down to where they either demise or impact the ground.

The remainder of this paper will summarize the methodology in both the MORSAT and ORSAT codes. The assumptions in the various parametric and spacecraft reentry analyses investigated will then be described. The principal results of the 6-month investigation will be presented, including a parametric study of spheres and cylinders of variable materials undergoing orbital decay. Variables for the spheres include mass, diameter, wall thickness, and ballistic coefficient. For the cylinders, four modes of tumbling and/or spinning were also considered.

In addition, the results of an orbital decay of the Delta rocket second-stage fragments including a stainless steel propellant tank and a titanium helium-pressurization sphere are presented. The results of orbital decay of aluminum and nickel alloy components of the Japanese NASDA Advanced Earth Observing Satellite (ADEOS)[7] are described. Finally, the orbital decay results of the Russian COSMOS 954 satellite[8,9] beryllium cylinders will be discussed.

Methodology

The details of the method of analysis in the MORSAT and ORSAT programs have been presented previously.[5,6] The specific input/output features of MORSAT are contained in the MORSAT 1.5 User's Manual.[4] Similarly, the detailed operational features of ORSAT are presented in the ORSAT 4.0 User's Manual.[3] A short summary of five general areas (models) of the code are presented below and are categorized as: trajectory/atmosphere model, aerodynamics model, aerothermodynamics model, thermal analysis and demise model, and reentry risk analysis model.

Trajectory/Atmospheric Model

Two options or initial conditions exist in the codes for trajectory analysis - targeted entry and entry from decaying orbit. The targeted entry permits the prediction of hardware impact locations on the Earth without assessing the reentry survivability (i.e., predicting the heating loads on the object). The most common mode of entry is orbital decay in which the heating loads and demise altitude may be computed, but not the actual impact points.

For either entry option, a 3-degree-of-freedom trajectory is computed using four equations derived in an Earth-fixed reference frame. These equations, which are derived assuming a spherical, rotating Earth, include the time-rate of change of altitude, longitude, relative velocity, and flight path angle. The components of the Earth's angular velocity expressed in the wind-axis system are contained in the equations. A fourth-order Runge-Kutta numerical integration scheme is used to solve the equations to obtain the object's altitude, relative velocity, flight path angle, and longitude at each time step.

The atmospheric model in the two codes is the 1976 Standard Atmosphere Model. Interpolation in this model produces the atmospheric density, pressure, temperature, speed of sound, and mean free path at each time step.

Aerodynamics Model

In the trajectory equation for relative velocity, there is a term which includes the drag force (with the drag coefficient, C_D). The drag coefficients in the codes are computed by various means, depending on the shape of the body (i.e., sphere, cylinder, flat plate, or box) and on the flow regime (continuum, transition, or free molecule) of the body at the particular time point. The details of all these drag coefficients have been discussed previously.[5]

For a sphere, the continuum drag coefficient is a constant at 0.92 for values of the Knudsen No., Kn (defined as mean free path divided by diameter), of less than 0.01. For spheres in the free molecular regime, where Kn >1.0, the drag coefficient is a constant value of 2.0. In the continuum regime, the value of C_D for spinning cylinders entering broadside is 1.22, and in free molecular flow, it is 2.0. For spinning cylinders entering end-on, tumbling end-over-end, or with random tumbling, the continuum and free molecular values of C_D are a function of the cylinder diameter divided by its length. The drag coefficient for a tumbling flat plate is 0.707 for continuum flow and 1.273 for free molecule flow. For tumbling boxes, these respective values are 1.42 and 2.55 (approximately twice those for a tumbling flat plate).

In the transition regime where $0.01 < Kn < 1.0$, a bridging function of C_D vs. Kn is used for spheres and broadside spinning cylinders. For tumbling cylinders, C_D is scaled to the variation for a sphere. For end-on cylinders, C_D varies linearly with Kn from the

continuum to free molecular regimes. Integral methods are used with a bridging function for tumbling flat plates and boxes.

Aerothermodynamics Model

The net heating rate to an object is equal to the hot wall heat rate (which is a function of the cold wall heat rate) plus the oxidation heat rate minus the reradiation heat rate. The cold wall convective stagnation point heating rate for spheres is based on the Detra, Kemp, and Riddell equation for continuum flow.[10] The free molecular heat rate is equal to one half the density times velocity cubed times an accommodation coefficient of 0.9. For Kn > 10, the free molecule value is used for the cold wall stagnation heat rate. For Kn < 0.001, the continuum value is used. For 0.01 < Kn < 10, the Stanton No. interpolated from empirical data is used. Finally, for 0.001 < Kn < 0.01, a power relation is used to determine the Stanton No.

The average cold wall heating rate is computed as the stagnation point heat rate for a sphere multiplied by a factor which accounts for the type of body (sphere, cylinder, flat plate, or box). The cylinder factors are a function of the diameter divided by the length of the cylinder for free molecular and continuum flow. In the transition regime, a variation of Stanton No. vs. Kn is used. For flat plates in free molecular flow, the Stanton No. is computed as a function of the speed ratio. For flat plates in continuum flow, a function of stagnation point heating to a sphere is used based on the length/width ratio of the plate. In the transition flow regime, an exponential bridging function is used for the flat plate. For boxes, the average cold wall heating rates use integral, empirical, and exponential bridging functions for free molecule, continuum, and transition flow, respectively.

The hot wall heat rate is equal to the cold wall value multiplied by the wall enthalpy ratio. The oxidation heat rate is based on an empirical constant times the cold wall heat rate times the oxide heat of formation as used in ORSAT. This term is currently not in the MORSAT code (to provide for a conservative situation or survivability of the object). Finally, the reradiation heat rate is a function of wall temperature to the 4th power times the material surface emittance. The higher the emittance, the lower the net heat rate, and better chance of object survival.

Thermal Analysis and Demise Model

Two methods are used to obtain the surface temperature and point of demise of the object. The first is the lumped mass model and is used with MORSAT because it is the quickest method to use. The net heat rate is integrated over time to obtain the heat load. The heat load is reduced by 60% for a sphere and by 33% for a cylinder to account for the progressively smaller size of the object, with a linear decrease in mass with time. The heat load is multiplied by the object surface area to obtain the total absorbed heat. The surface temperature at any time is computed as the initial temperature plus the total absorbed heat divided by the object mass times its specific heat. After the melting temperature is reached, the surface temperature is held constant until the absorbed heat reaches the material heat of ablation. This heat of ablation is defined as the sum of the mass times the heat of fusion of the material plus the melt - initial temperature difference times the mass times specific heat. At this point, the object is considered to burn up or demise. However, if the absorbed heat never reaches the heat of ablation, the object will not burn up even though it has exceeded its melting temperature.

The second method of predicting surface temperature or point of demise is the nodal thermal math model which is used only with ORSAT. The 1-D heat conduction equation is solved by using a forward-time-central-space finite difference solution in spherical or cylindrical coordinates for up to 20 nodes in the model. Multiple types of material may be incorporated in the model with thermal conductivity input as a function of temperature. After the absorbed heat reaches the heat of ablation of the outer layer, the layer is removed by an assumed shear force, and the net heat rate is applied to the next layer. The mass and diameter change after each layer removal. The process continues until all layers reach their respective heat of ablation based on the decreased mass after each layer is removed. Unlike MORSAT, the surface temperature may drop after the melting temperature is removed if the net heat rate to the surface is decreasing.

Reentry Risk Analysis Model

In MORSAT, for objects that survive reentry, the debris area is computed by using the maximum cross sectional area of the object and adding a 0.3 m border around the object. The total debris area equals the sum of the individual fragment areas that have broken off the original parent body. The expected number of casualties (i.e., risk) equals the probability of impact on land mass

times the population of the land area in the latitude band times the debris area divided by the land area.

Assumptions in Analyses

Parametric Study

The MORSAT code was used to predict entry heating rates and loads, absorbed heats, temperatures, demise altitude, and/or survivability of metallic spheres and cylinders. Five materials were considered in this analysis: aluminum, copper, stainless steel, titanium, and beryllium. Three object variables were considered: thickness (0 - 100 mm), diameter (0.05 - 1.0 m), mass (0.1 - 30 kg), ballistic coefficient (10 - 1000 kg/m^2), and surface emittance of 1.0 and 0.3. Both solid and hollow spinning spheres were evaluated. Hollow cylinders of 3.0 m length with a 0.5 m diameter were considered with four modes of entry. These included end-on spinning (no tumbling), random tumbling and spinning, broadside spinning (no tumbling), and end-over-end tumbling and spinning.

A parent object for all fragments consisting of a sphere of diameter of 1.852 m with a mass of 1300 kg was used based on an example (SPARTAN spacecraft) in the user's manuals.[3,4] A breakup altitude of 78 km was assumed for all objects. In some cases, results from ORSAT were used to compare with those of MORSAT.

Delta 2nd Stage

The Delta II rocket was launched on April 24, 1996 to deliver a Ballistic Missile Defense Organization (BMDO) Midcourse Space Experiment (MSX) payload to orbit. On January 22, 1997, the 2nd stage of the Delta rocket reentered the atmosphere. Two fragments survived entry: a stainless steel cylindrical propellant tank which landed near Georgetown, Texas and a titanium helium-pressurization sphere which landed near Seguin, Texas. Post-flight photographs of these cylindrical and spherical fragments are shown in Figs. 1 and 2, respectively. The cylinder showed evidence of surface melting; however, the sphere did not, with only some slight discoloring.

The MORSAT and ORSAT codes were run to determine the entry conditions and survivability of the two fragments. The parent body was assumed to be the Delta 2nd stage empty cylindrical tank with a length of 5.97 m, diameter of 2.44 m, and mass of 919 kg as seen in Fig. 3a. Figure 3b presents a pre-flight photo of this stage showing the pressurized spheres and the engine on the left of the photo. Initial dimensions of the stainless steel cylinder which survived were obtained at the NASA/JSC shipping and receiving area and were later adjusted with better measurements obtained from McDonnell Douglas as shown in Fig. 4. Originally, the initial breakup altitude was assumed to be 78 km. However, a later reconstructed best-estimate trajectory was furnished by Aerospace Corp., and was used to establish initial conditions at breakup. From this trajectory, the breakup altitude was determined to be 80.58 km, with a relative velocity of 7668 m/sec, an inclination angle of 96.6°, and a relative flight path angle of -0.545°.

From Fig. 4, the diameter of the stainless steel cylinder was determined to be 1.742 m. An average thickness was determined to be 1.49 mm, resulting in an inner radius of 0.8696 m and outer radius of 0.8711 m. An effective length was determined to be 1.853 m assuming an effective length of the hemispherical end caps was one half the radii. This is because the codes only model flat-faced cylinders and not cylinders with hemispherical end caps. A mass of 267 kg as obtained from McDonnell Douglas was used for the cylinder. The titanium sphere was weighed at JSC to be 30.6 kg, with a sphere diameter of 0.60 m. Using the density of titanium as 4437 kg/m^3, an average thickness of 6.3 mm was obtained. Surface emittances of 1.0 and 0.3 were considered for both fragment materials. Three nodes were used in the ORSAT thermal analysis.

ADEOS

The National Space Development Agency (NASDA) of Japan launched the ADEOS satellite (seen in the sketch of Fig. 5) aboard a Japanese H2 rocket on Aug. 17, 1996. In a document[7] NASDA described an analysis of survivability of various ADEOS fragments after the breakup of the parent body satellite as it undergoes a hypothetical orbital decay reentry.

This NASDA ADEOS analysis was evaluated, and an independent, similar reentry survivability study was performed using MORSAT for two ADEOS fragments: the Advanced Visible and Near Infrared Radiometer (AVNIR) unit and the EPS unit battery. Most of the assumptions used by MORSAT described below were contained in the NASDA document.[7] The parent body before breakup was assumed to be a spinning cylinder entering broadside with a diameter of 4.5 m, a length of 5.0 m, and a mass of 3000 kg. The altitude at breakup of the parent body was assumed to be 80 km.

The two fragments (AVNIR and EPS battery) were considered to be random tumbling rectangular parallelepipeds (boxes). The AVNIR had dimensions of 1.0 m x 1.0 m x 0.4 m with a mass of 250 kg. The EPS battery had dimensions of 0.22 m x 0.26 m x 0.29 m with a mass of 46.7 kg. Two values of wall emittance of the AVNIR were considered: 0.2 and 0.9, while that of the EPS battery was assumed to be 0.85. The AVNIR material was an aluminum alloy, and the EPS battery material was a nickel alloy. The initial wall temperature of the AVNIR was 773 K and that of the EPS battery was 273 K.

COSMOS 954

The Russian COSMOS 954 satellite was launched on Sept. 18, 1977 and crashed in the Northwest Territories of Canada on Jan. 24, 1978.[8] A total of 49 pieces of beryllium fragments from this satellite were found on the ground. Included in this debris were 33 beryllium rods about 2 cm in diameter and 10 cm long, weighing about 50 - 60 g each and six larger solid beryllium cylinders about 10 cm in diameter and 40 cm long, weighing about 3600 g each. These larger cylinders were investigated with the MORSAT code using the random tumbling and spinning option.

The parent body was considered to be a cylinder of 1.3 m dia., 5.8 m length, and 1250 kg mass.[9] This cylinder was assumed to be a spinning body entering broadside with breakup occurring at 78 km. The initial wall temperature was taken as 300 K, and a wall emittance for beryllium was assumed to be 0.3.

Results

Parametric Analysis

Figure 6 presents a plot of the demise altitude from MORSAT as a function of the mass of solid spheres. Five materials were considered in the study: copper, aluminum, stainless steel, titanium, and beryllium. However, beryllium survived for all values of mass and is not shown on the plot. The survivability points on this figure are the points slightly beyond the highest mass for each material (i.e., if the aluminum sphere mass is greater than 16 kg, it will survive). It is seen that copper has the highest mass at the survival point, followed by aluminum, stainless steel, and titanium.

In Fig. 7 the demise altitude is plotted as a function of the diameter of solid spheres using MORSAT. The same five materials were considered as for Fig. 6. However, beryllium spheres survived even at the smallest diameters. It is seen that for the same diameter, aluminum spheres burn up at higher altitudes, followed by copper, stainless steel, and titanium spheres.

Figure 8 presents the demise altitude as a function of sphere thickness for a 0.05 m dia. hollow sphere of various materials using MORSAT. The demise altitude appears to flatten out as the thickness reaches the value for a solid sphere (25 mm). It is seen that for aluminum, copper, and stainless steel spheres, as the thickness decreases, a higher demise altitude is reached. However, for titanium, the hollow sphere reaches a peak demise altitude around 5 mm thickness, but at lower thickness, this altitude decreases until for values less than 0.3 mm, it survives. Also, for beryllium hollow spheres, the object survives for all values of thickness.

In Fig. 9 the results of Fig. 8 are shown as a function of ballistic coefficient, W/C_DA, where W is the weight (mass) of the hollow sphere and A is the cross-section area of the 0.05 m diameter sphere. Since the flow regime is near continuum ($Kn < 0.01$), the drag coefficient is around 0.92. The cross section area is a constant, so the primary variable in ballistic coefficient is the mass, which is computed as the product of material density times volume of the sphere (based on the thickness). The trends of this plot for a 0.05 m diameter sphere are similar to those of Fig. 8, with the titanium sphere beginning to survive at the low thicknesses. The value on the right of each curve represents the maximum thickness (or solid sphere).

Figure 10 presents a similar plot to Fig. 9 with the demise altitude plotted as a function of ballistic coefficient, but for a diameter of 0.20 m. In this figure only three curves are shown, as the titanium sphere survives for all values of ballistic coefficient. Also, it is seen that the stainless steel begins to survive at low values of ballistic coefficient (similar to the titanium sphere in Fig. 9). The values on the right of the copper and stainless steel curve also show the beginning of survivability. For a larger diameter of 0.3 m (not shown), the stainless steel sphere survived at all values of ballistic coefficient, and only the aluminum and copper spheres burned up.

In Figs. 9 and 10, the demise altitude drops as the ballistic coefficient increases. This is in contrast to the plot shown in Refs. 5 and 6 for demise altitude increasing with ballistic coefficient. However, in these references, this plot was for a fixed thermal mass with the thickness maintained constant at 3 mm with ballast

added to the sphere to increase the aerodynamic mass and the ballistic coefficient. In Figs. 9 and 10, the thermal mass is the same as the aerodynamic mass with ballistic coefficient varying with the wall thickness.

In Fig. 11, the demise altitude is shown as a function of sphere thickness for an aluminum sphere of various diameters. The 0.1 m dia. sphere (like the 0.05 m dia. sphere in Fig. 8) burns up at all thicknesses. Each larger sphere survives at decreasing thicknesses. The 1.0 m dia. aluminum sphere survives at thicknesses greater than only 3 mm.

Figures 12 and 13 present the demise altitude as a function of cylinder thickness for 0.5 m diameter, 3.0 m long aluminum and copper cylinders, respectively. It is seen that the end-on spinning case has the highest altitude of demise because the heating is applied only on the front face and not distributed over the body like the other modes. Using the other three modes of entry, the cylinders survive around the same altitude (35 - 42 km). For the same thickness, the aluminum cylinders burn up at a higher altitude than the copper cylinders. Stainless steel and titanium cylinders survive (not shown in this plots), even at the lowest thickness, except for the end-on mode where they burn up around 75 km and higher.

In Fig. 14 the heat of ablation and absorbed heat to a 0.10 m dia. aluminum sphere is plotted as a function of altitude for 5 thicknesses from 2.5 mm to 50 mm. When the absorbed heat reaches the heat of ablation, this altitude is the demise altitude. The change in slope occurs when the surface temperature reaches the melting temperature and the reradiation heat rate is a constant. These temperatures are shown in Fig. 15 for the same size sphere and thicknesses.

Delta 2nd Stage

Figure 16 shows the ORSAT-predicted heating rate components (cold wall, hot wall, net, oxidation, and reradiation) to the Delta 2nd stage titanium sphere. An oxidation heating factor of 1.0 (maximum value) was used in this analysis. The peak cold wall heat rate is about 35 W/cm^2 and drops significantly after about 100 sec. After the net heat rate reaches zero, the reradiation heat rate drops. The stainless steel cylinder heat rate components are shown in Fig. 17. An oxidation heating factor of only 0.4 could be used before the cylinder survived. The reradiation heat rate stays at a constant value from 50 to 150 sec because this is at the melt temperature of stainless steel.

Figures 18 and 19 show the surface temperatures on the Delta sphere and cylinder as a function of time. Both of these cases used a surface emittance of 0.3. If a value of 1.0 had been used, the temperature and reradiation heat rate would have been lower. The titanium sphere was within 100 K of its melt temperature of 1943 K; however, the stainless steel cylinder reached its melt temperature of 1728 K and stayed there for about 100 sec. From visible observation of the cylinder, it was evident that the cylinder surface had melted on one end (yet it survived).

In Figs. 20, 21, and 22, the altitude, relative velocity, and flight path angle are plotted as a function of downrange from the breakup point. It is seen that the sphere landed about 170 km further than the cylinder. The relative distance between Georgetown and Seguin, Texas is about 135 km; hence, the difference in predicted downrange is somewhat close to the actual value. The sphere is traveling at a faster velocity, higher altitude, and less negative flight path angle. Thus, the sphere would be expected to land at a farther location than the cylinder.

ADEOS

Figures 23 and 24 show the heating rate components to the aluminum AVNIR and EPS battery, respectively, vs. time. The net heat rate is higher with emittance of 0.2 than 0.9, with the reradiation heat rate higher at 0.9. The heating rates to the EPS battery are more than twice as high for the AVNIR because of the smaller dimensions of the AVNIR. Since MORSAT was used, no oxidation heating was considered.

In Figs. 25 and 26 the absorbed heat and heat of ablation for the aluminum AVNIR and nickel EPS battery are shown, respectively. Since the heat of ablation is not reached in either case, the objects survived (same as the NASDA analysis). The melt temperatures of each material are reached in the MORSAT analysis; however, these temperatures were not reached in the NASDA analysis.

The debris casualty area computed by MORSAT was 2.56 and 0.77 m^2 for the AVNIR and EPS battery, respectively. This is comparable to the values reported in the NASDA analysis.

COSMOS 954

Figure 27 presents the heating components vs. time for the beryllium cylinder for the COSMOS 954 entry.

Because of the small size of this cylinder, the heating rates were very high - 96 W/cm^2 for the cold wall value and 90 W/cm^2 for the net value. As with the ADEOS cases, no oxidation heating was used with MORSAT. Although the time of impact to the ground was 510 sec, the plot was stopped at 300 sec for clarity.

In Figure 28 the absorbed heat and heat of ablation to the beryllium cylinder are presented. It is seen that the absorbed heat never reaches the heat of ablation of beryllium even though the heating rates are so high. This is because of the extremely high heat of fusion of beryllium (nearly three times higher than that of titanium). The peak surface temperature was 1446 K (not shown), which was 111 K lower than the beryllium melting temperature of 1557 K.

Conclusions

This six-month study sponsored by NASA/JSC has investigated reentry heating, demise altitude, and/or survivability of spacecraft objects undergoing orbital decay. The study used the JSC MORSAT and ORSAT codes for the reentry analysis. The parametric analysis for spheres and cylinders assessed effects of variable thickness, diameter, ballistic coefficient, and material, plus effects of spinning and tumbling for cylinders. In general, aluminum and copper objects tend to burn up in the atmosphere, whereas beryllium, stainless steel, titanium, and nickel objects tend to survive. Two fragments of the Delta 2nd stage rocket were investigated and were predicted to survive and land within 35 km of the actual difference in location between impact points (Georgetown and Seguin, Texas). Predictions for the two NASDA ADEOS fragments showed the objects survived entry, as did the analysis for the COSMOS 954 beryllium cylinders which landed in Canada. The methods used in this study may be applied to almost all existing or future satellites to establish their survivability during entry and risk to human life and property on the ground.

Acknowledgments

The authors wish to acknowledge the help of Chris Madden (NASA/JSC), Stan Bouslog (Rohr, Inc.), Brian Ross (NASA/Goddard), and K. C. Wang (Lockheed Martin - Skunk Works) who were the original developers of the MORSAT and ORSAT orbital debris reentry codes. Thanks are also extended to Bill Ailor (Aerospace Corp.) who provided the COSMOS 954 data and other information, and to Benjamin Mains (Aerospace Corp.) who supplied the Delta 2nd stage reconstructed best-estimate trajectory for the cylindrical and spherical tanks.

References

1. "Interagency Report on Orbital Debris," Executive Office of the President of the United States, The National Science and Technology Council Committee on Transportation Research and Development, 1995.

2. "NASA Safety Standard Guidelines and Assessment Procedures for Limiting Orbital Debris," NSS 1740.14, August 1995.

3. Ross, B. P., Madden, C. B., and Bouslog, S. A., "A User's Guide for the Object Re-entry Survival Analysis Tool (ORSAT) Version 4.0," JSC-26311, August 1993.

4. Bouslog, S. A., Ross, B. P., and Madden, C. B., "User's Guide for Miniature - ORSAT (Object Reentry Survival Analysis Tool): MORSAT - Version 1.5," JSC-26869, Rev. A, September 1995.

5. Bouslog, S. A., Wang, K.-C., Ross, B. P., and Madden, C. B., "Reentry Survivability and Risk Analysis," JSC-27232, September 1995.

6. Bouslog, S. A., Ross, B. P., and Madden, C. B., "Space Debris Reentry Risk Analysis," Paper 94-0591 presented at 32nd Aerospace Sciences Meeting, Reno, NV, Jan. 10-13, 1994.

7. Harashima, O., "Actions Items of NASA/NASDA 5th W. G. Meeting on M. S. A., including attachment, 'The Study of the Casualty Area Due to the Debris Surviving,'" Letter to Wayne R. Frazier, NASA/HQ, Code QS, N97-411-1, April 11, 1997.

8. Hanafee, J. E., "Analysis of Beryllium Parts for COSMOS 954," Lawrence Livermore Laboratory UCRL-52597, Oct. 25, 1978.

9. "Use of Nuclear Power Sources in Outer Space," Report A/AC.105/C.1/WG.5/L.24/ADD.2, Committee on the Peaceful Uses of Outer Space, General Assembly United Nations, Feb. 26, 1990.

10. Detra, R. W., Kemp, N. H., and Riddell, F. R., "Addendum to 'Heat Transfer to Satellite Vehicles Re-entering the Atmosphere,'" *Jet Propulsion*, Vol. 27, No. 12, Dec. 1957.

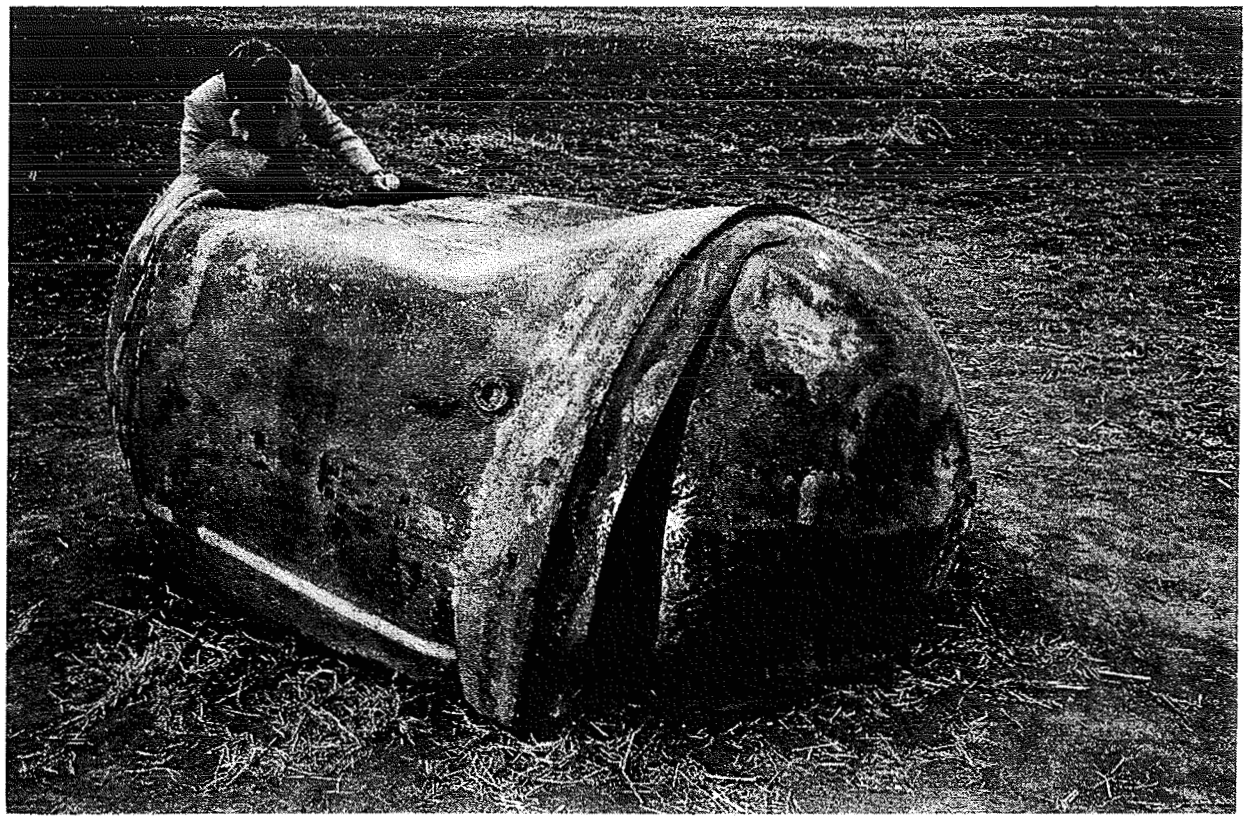

Fig. 1 Delta 2nd Stage Stainless Steel Cylinder Propellant Tank at Impact Point near Georgetown, TX

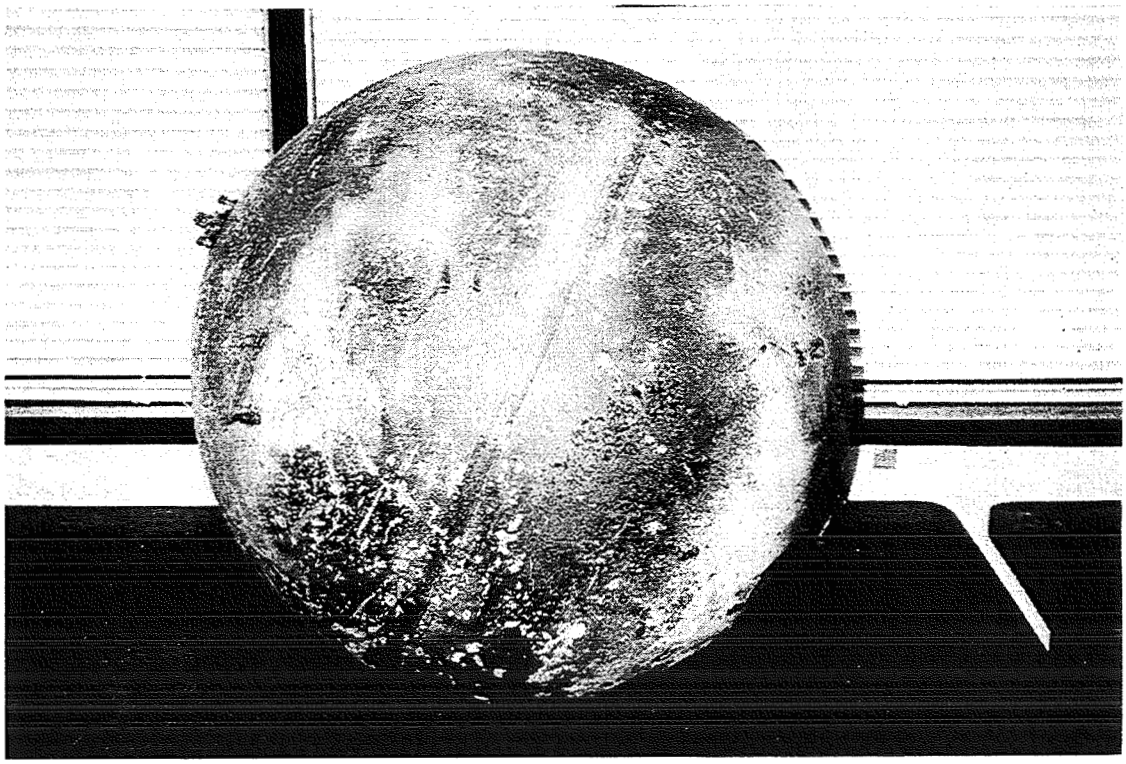

Fig. 2 Delta 2nd Stage Titanium Helium-Pressurization Sphere which Landed near Seguin, TX

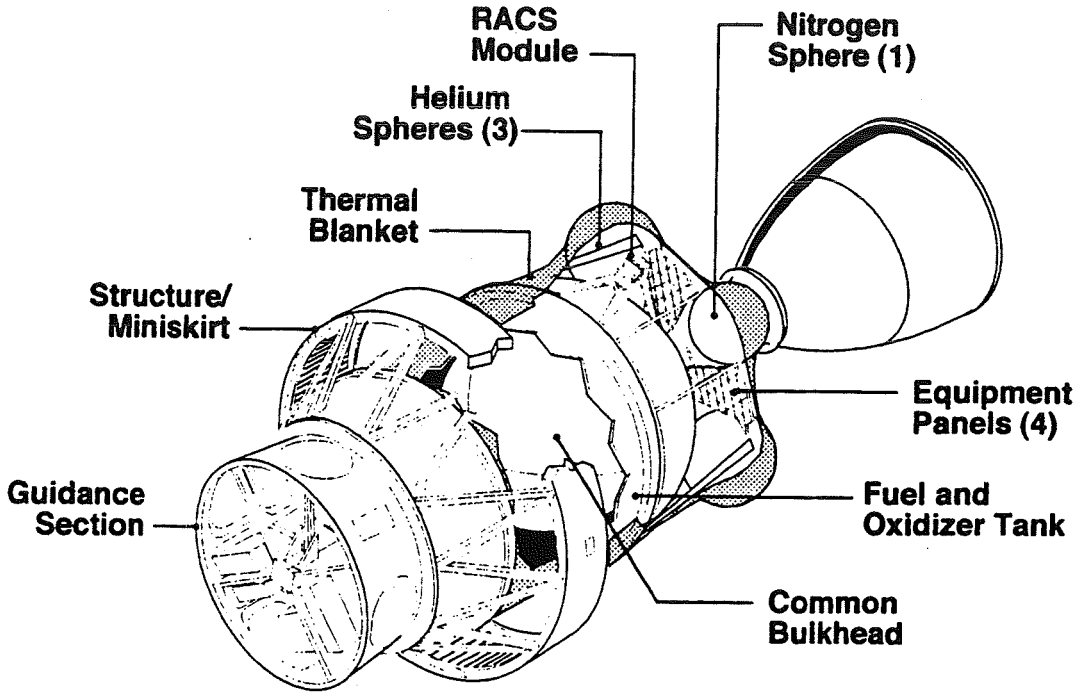

Fig. 3a Sketch of Delta 2nd Stage Assembly

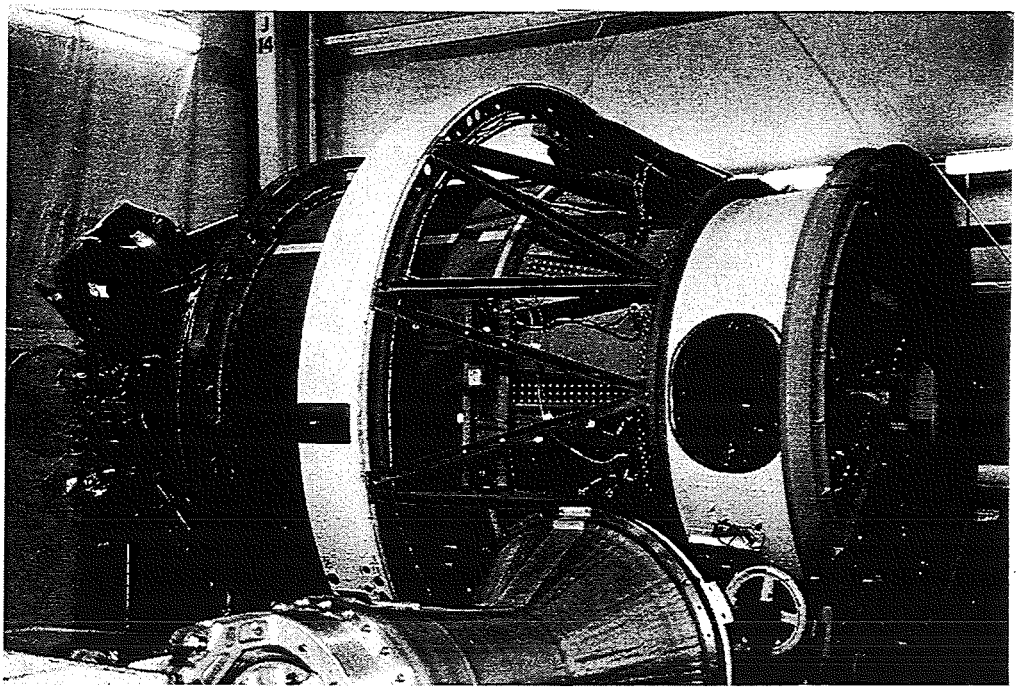

Fig. 3b Pre-Flight Photograph of Delta 2nd Stage Assembly

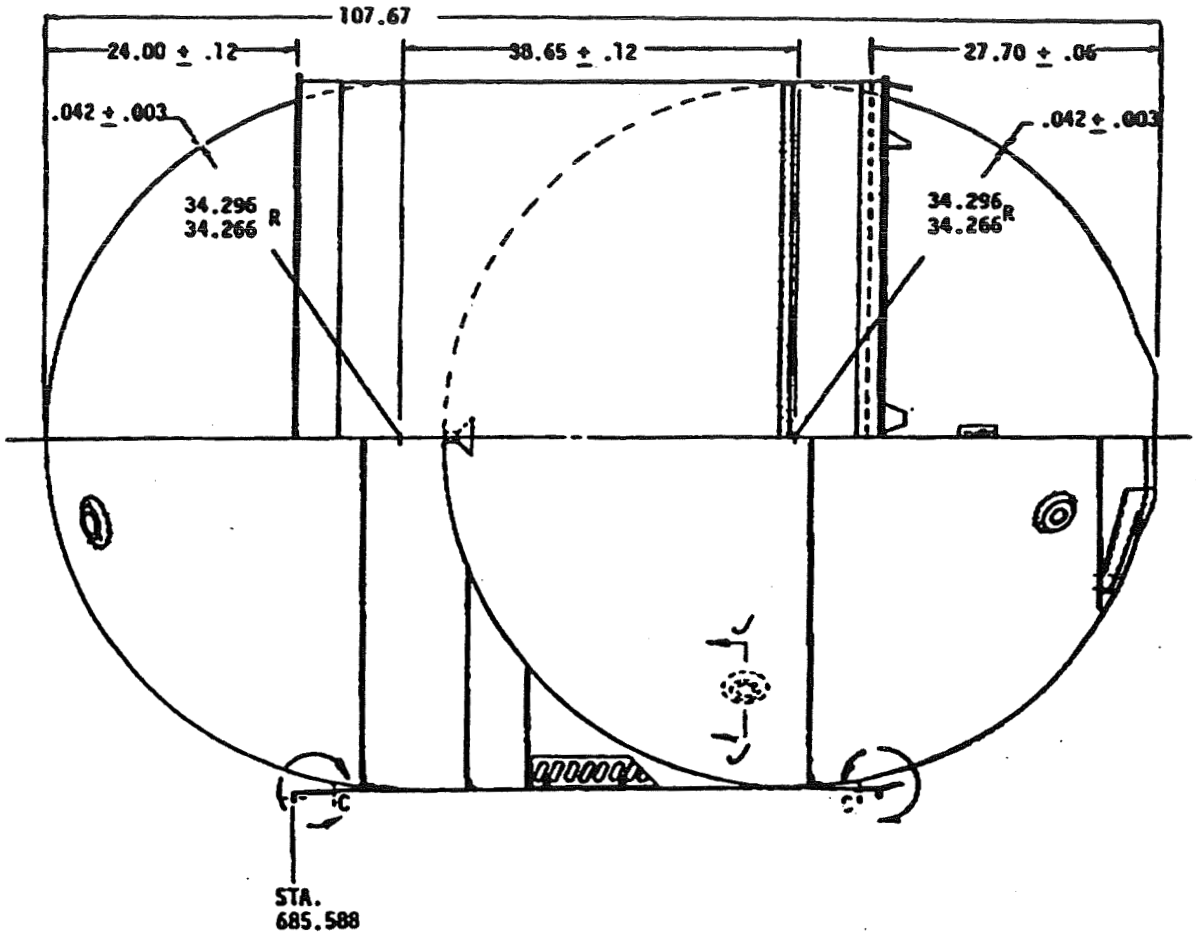

Fig. 4 Dimensions of Delta 2nd Stage Stainless Steel Cylindrical Propellant Tank

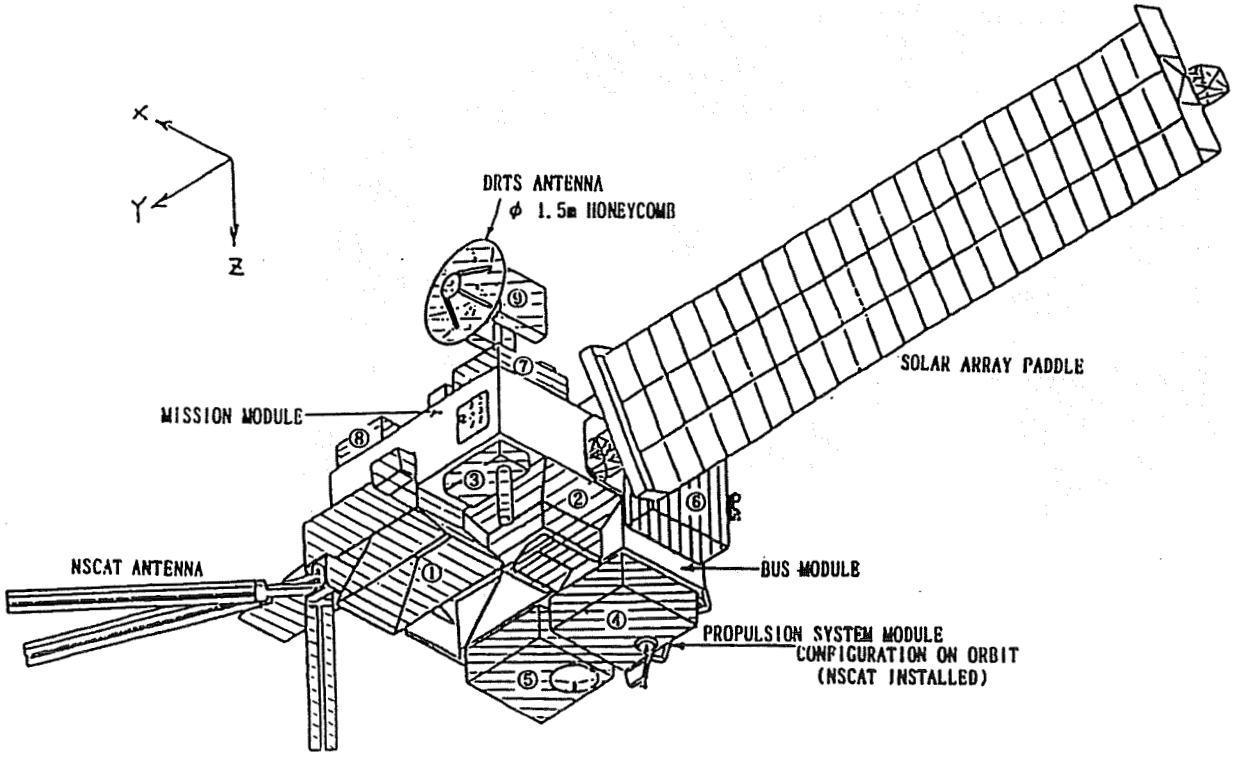

Fig. 5 Japanese Advanced Earth Observing Satellite (ADEOS) Configuration

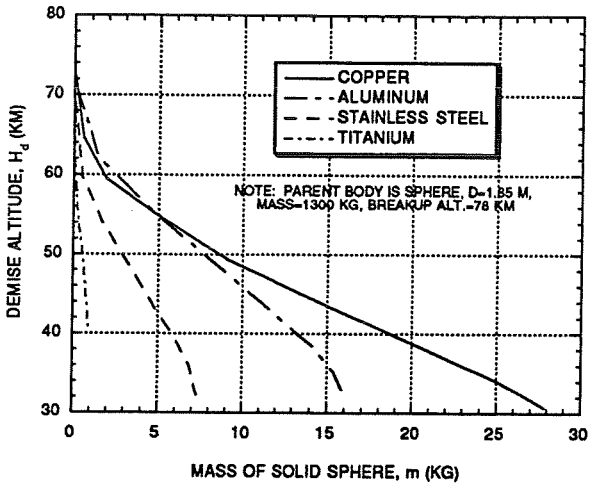

Fig. 6 Demise Altitude vs. Mass for Solid Sphere of Various Materials

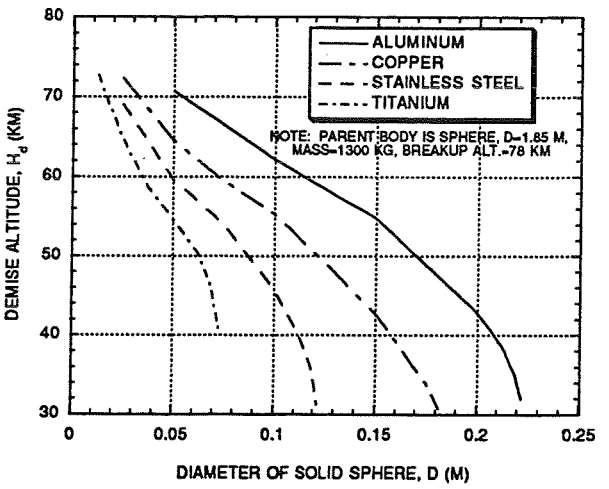

Fig. 7 Demise Altitude vs. Diameter for Solid Spheres of Various Materials

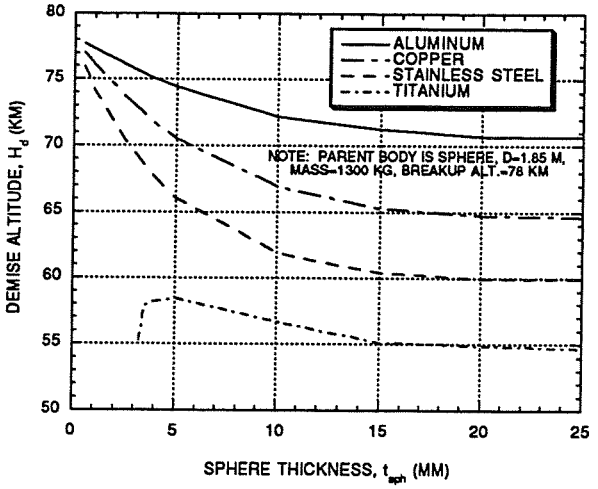

Fig. 8 Demise Altitude vs. Sphere Thickness for 0.05 m Dia. Sphere of Various Materials

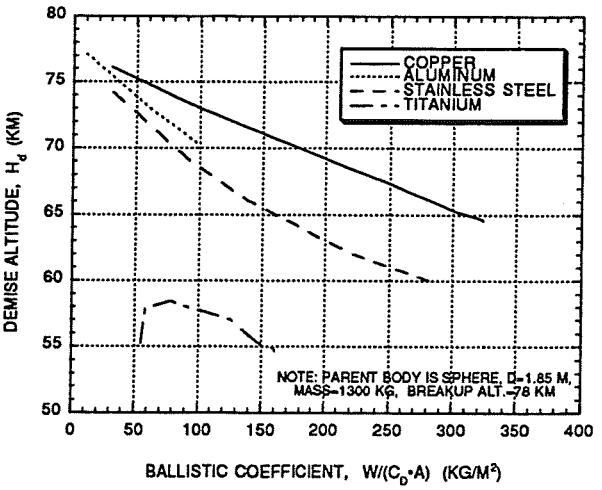

Fig. 9 Demise Altitude vs. Ballistic Coefficient for 0.05 m Dia. Sphere of Various Materials

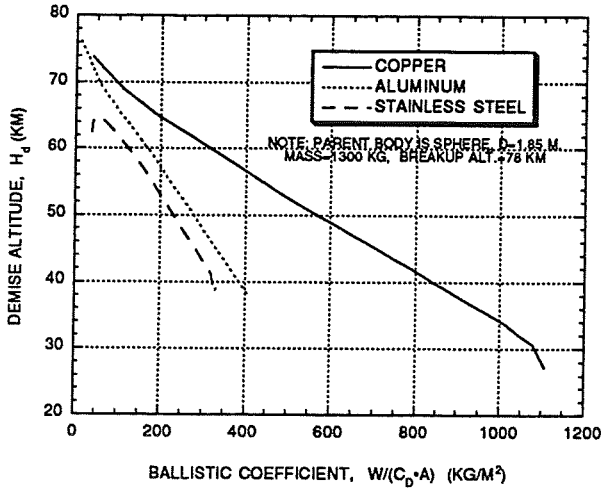

Fig. 10 Demise Altitude vs. Ballistic Coefficient for 0.20 m Dia. Sphere of Various Materials

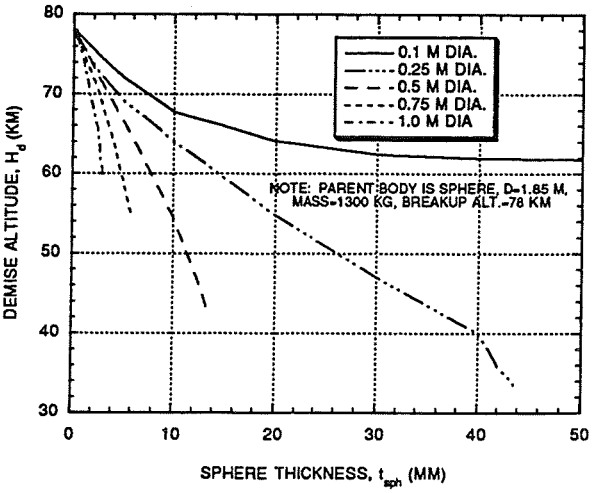

Fig. 11 Demise Altitude vs. Sphere Thickness for Aluminum Sphere of Various Diameters

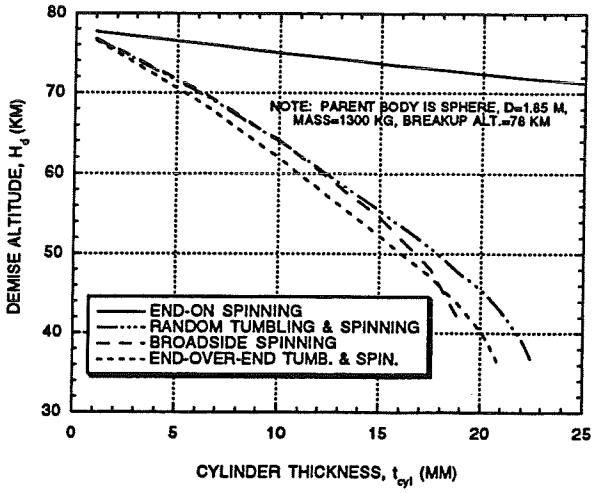

Fig. 12 Demise Altitude vs. Cylinder Thickness for 0.5 m Dia., 3.0 m Long Aluminum Cyl.

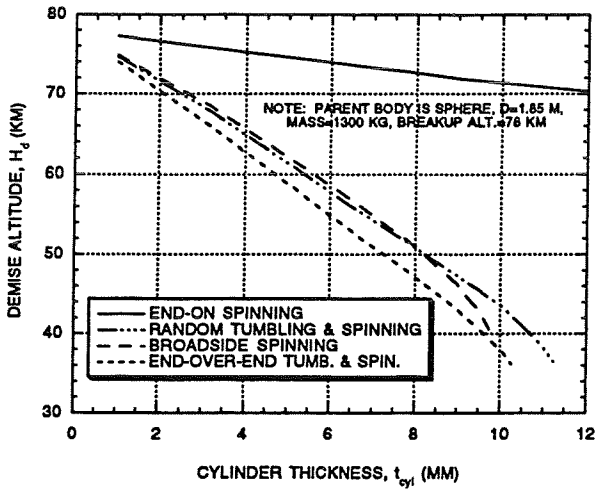

Fig. 13 Demise Altitude vs. Cylinder Thickness for 0.5 m Dia, 3.0 m Long Copper Cylinder

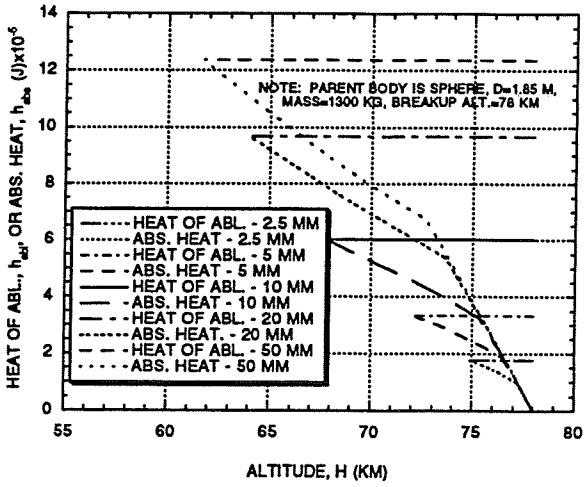

Fig. 14 Heat of Ablation & Absorbed Heat to 0.10 m Dia. Al Sphere for Various Thick. vs. Alt.

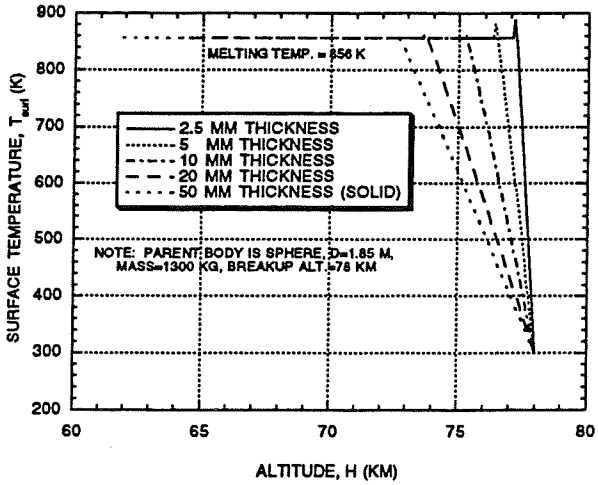

Fig. 15 Surface Temperature on 0.10 m Dia. Al Sphere for Various Thicknesses vs. Altitude

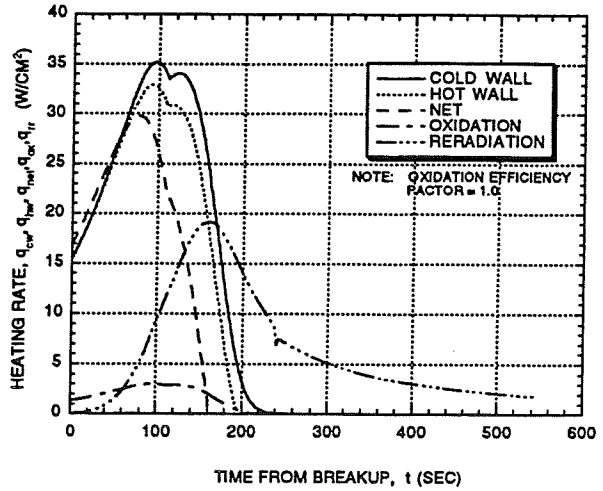

Fig. 16 Heating Rate Components to Delta 2nd Stage Titanium Sphere vs. Time from Breakup

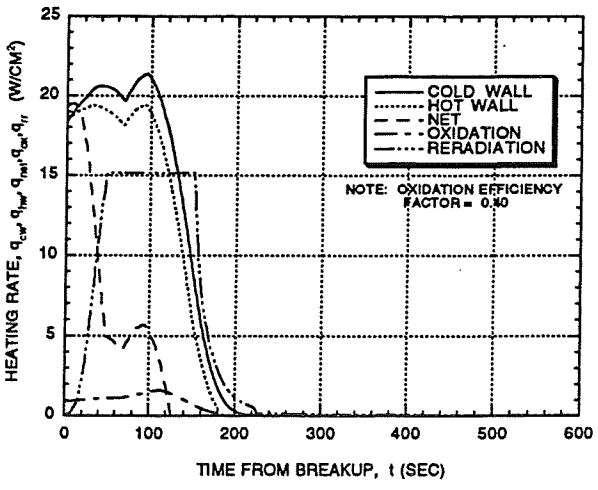

Fig. 17 Heating Rate Components to Delta 2nd Stage Stainless Steel Cyl. vs. Time from Breakup

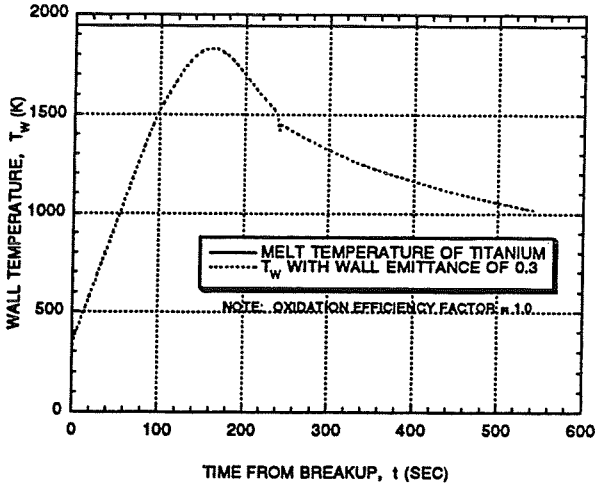

Fig. 18 Wall Temperature for Delta 2nd Stage Titanium Sphere vs. Time from Breakup

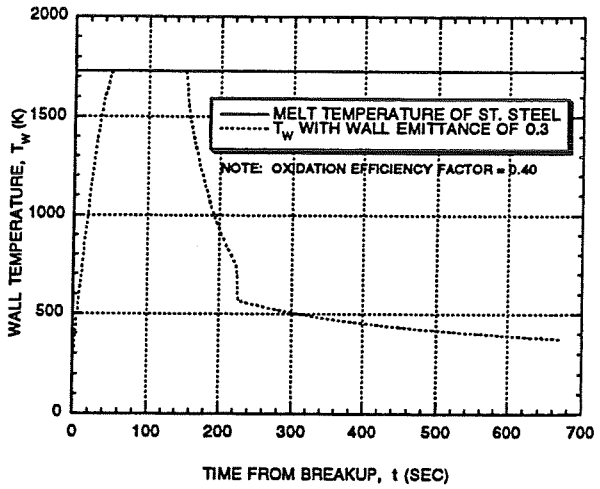

Fig. 19 Wall Temperature for Delta 2nd Stage Stainless Steel Cyl. vs. Time from Breakup

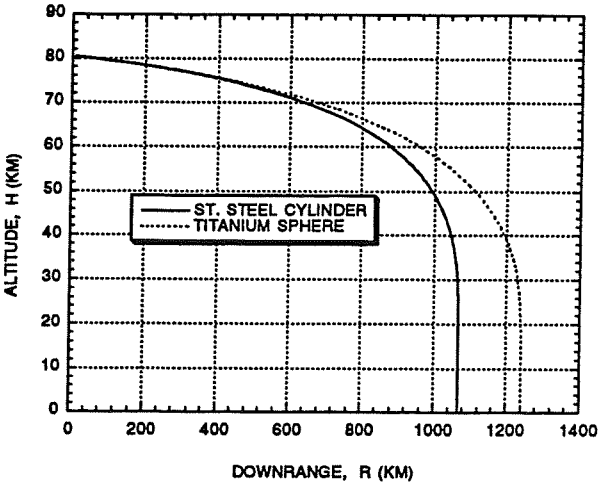

Fig. 20 Altitude for Delta 2nd Stage Fragments vs. Downrange

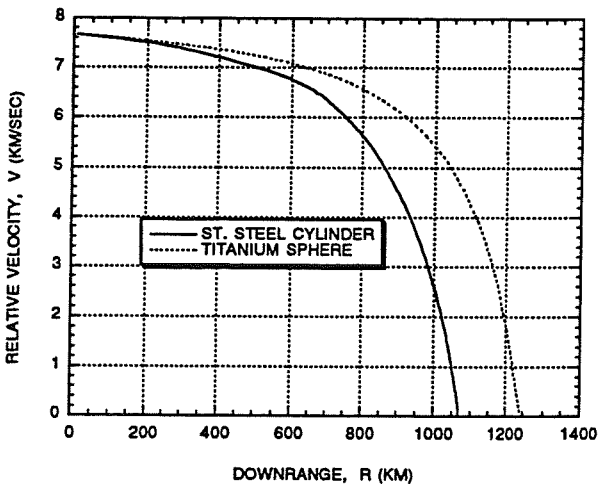

Fig. 21 Relative Velocity for Delta 2nd Stage Fragments vs. Downrange

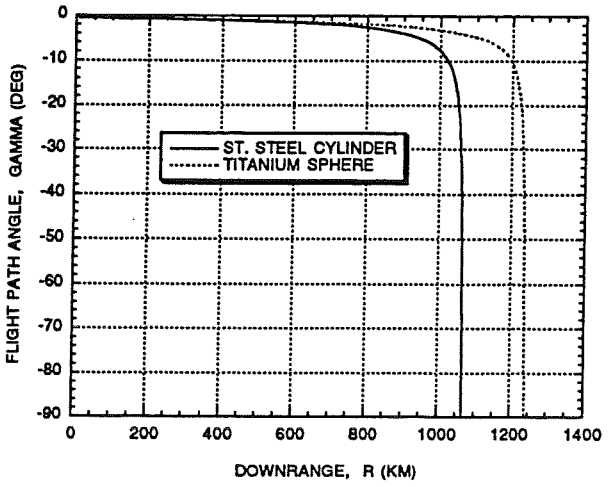

Fig. 22 Flight Path Angle for Delta 2nd Stage Fragments vs. Downrange

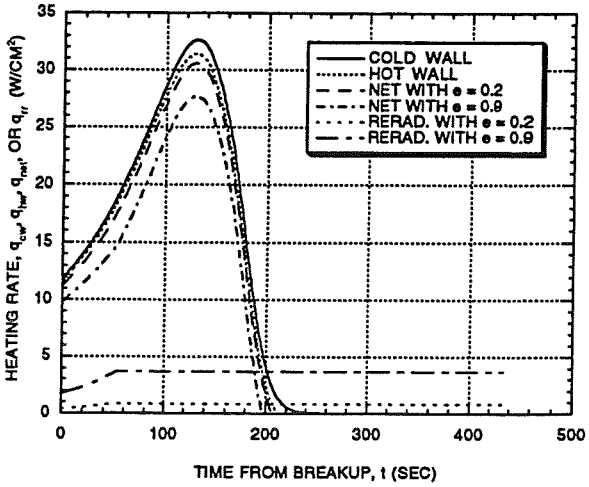

Fig. 23 Heating Rate Components to ADEOS Al AVNIR Box vs. Time from Breakup

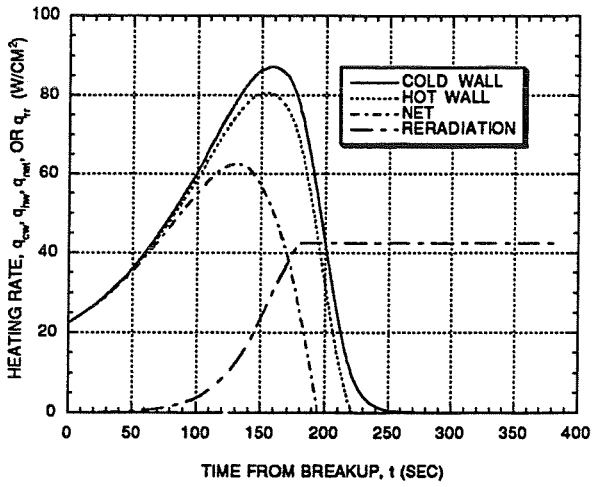

Fig. 24 Heating Rate Components to ADEOS Nickel EPS Battery Box vs. Time from Breakup

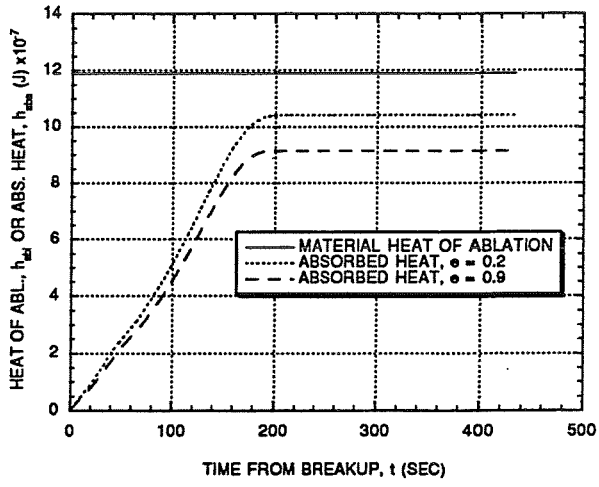

Fig. 25 Heat of Ablation & Absorbed Heat to ADEOS Al AVNIR Box vs. Time from Breakup

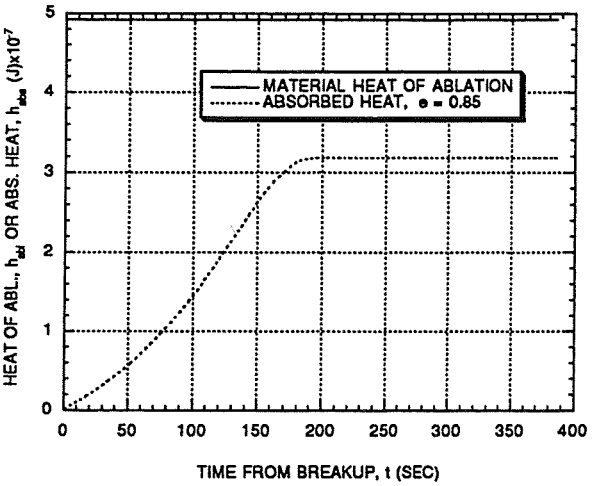

Fig. 26 Heat of Ablation & Absorbed Heat to ADEOS EPS Battery Box vs. Time from Breakup

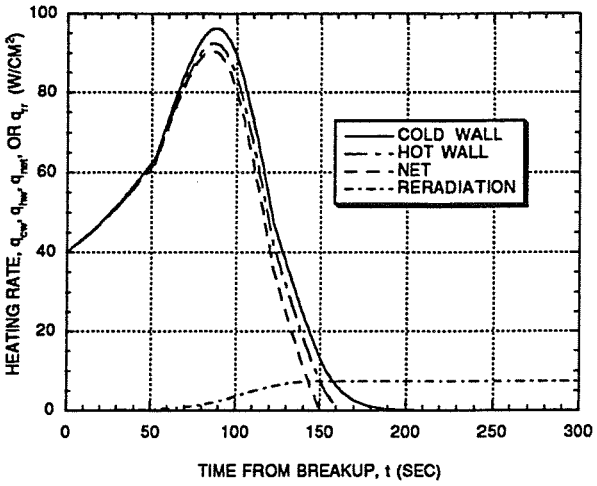

Fig. 27 Heating Rate Components to COSMOS 954 Beryllium Cylinder vs. Time from Breakup

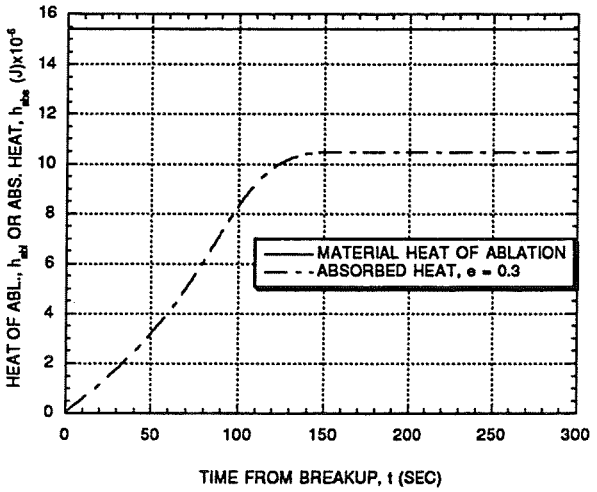

Fig. 28 Heat of Ablation & Absorbed Heat for COSMOS 954 Be Cyl. vs. Time from Breakup